ACS APPLIED MATERIALS & INTERFACES

Research Article

Cite This: ACS Appl. Mater. Interfaces 2017, 9, 44792−44798

www.acsami.org

Programmable and Shape-Memorizing Information Carriers

Wenbing Li,[†] Yanju Liu,[‡] and Jinsong Leng*[,†]

[†]Centre for Composite Materials and Structures, Harbin Institute of Technology (HIT), No. 2 YiKuang Street, P.O. Box 3011, Harbin 150080, PR China

[‡]Department of Astronautical Science and Mechanics, Harbin Institute of Technology (HIT), Harbin 150001, PR China

Supporting Information

ABSTRACT: Shape memory polymers (SMPs) are expected to play more and more important roles in space-deployable structures, smart actuators, and other high-tech areas. Nevertheless, because of the difficulties in fabrication and the programmability of temporary shape recovery, SMPs have not yet been widely applied in real fields. It is ideal to incorporate the different independent functional building blocks into a material. Herein, we designed a simple method to incorporate four functional building blocks: a neat epoxy-based shape memory (neat SMEP) resin, an SMEP composited with Fe_3O_4 (SMEP−Fe_3O_4), an SMEP composited with multiwalled carbon nanotubes, and an SMEP composited with *p*-aminodiphenylimide into a multicomposite, in which the four region surfaces could be programmed with different language code patterns according to a preset command by imprint lithography. Then, we aimed to reprogram the initially raised code patterns into temporary flat patterns using programming mold that, when triggered by a preset stimulus process such as an alternating magnetic field, radiofrequency field, 365 nm UV, and direct heating, could transform these language codes into the information passed by the customer. The concept introduced here will be applied to other available SMPs and provide a practical method to realize the information delivery.

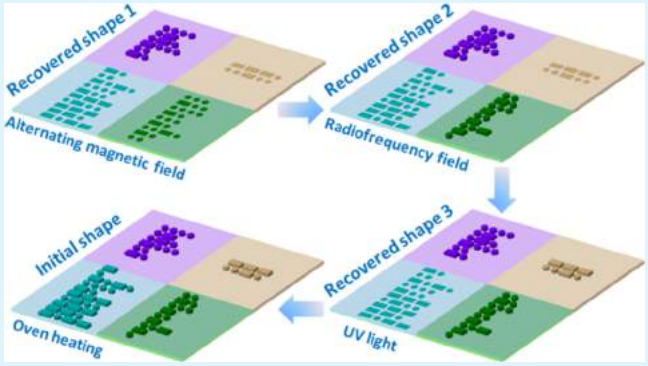

KEYWORDS: *programmable pattern memory, information delivery, selective actuations, multicomposite*

1. INTRODUCTION

Morse code is a preliminary encoding program for language in which the characters are transformed into dots (".") and dashes ("-").[1,2] Therefore, Morse code lies on the characters of letters but encodes them by unique sequences of "." and "-". Morse code as the language code itself is not a language but can represent or encode a given language, such as English. It is analogous to the handwriting, which can express the thoughts by means of words. Hence, for various reasons, the process of learning to transmit and identify these individual characters of Morse code has been of interest to researchers since the previous reports of Bryan and Harter.[3,4]

As one of the most important kinds of stimuli-responsive polymers, shape memory polymers (SMPs) can recover to their original shapes from deformed shapes when exposed to external stimuli.[5−16] This remarkable capability makes them excellent candidates for a broad range of applications, such as biomedicine, textile, aerospace, information carriers, flexible electronics, and so forth.[17−24] Currently, the most widely explored SMPs can recover under direct heating[25,26] or remote triggering[27,28] and cannot recover programmatically through a programmatic stimulus. On many occasions, this actuation mechanism is not practical when only the presupposed part of the material needs shape change.

The above-mentioned actuation mechanism that is used to trigger the shape recovery of SMPs is a limit to creating materials with advanced functionality and attractive applicability. Multicomposite SMPs made of multiple functional building blocks and combined with different driving methods could be used for the development of programmable useful functional materials. A number of such programmable polymers have been proposed recently, such as a dual-composite polymer which is the simplest form of such a construction and could be programmatically triggered in two steps;[29] a triple-composite polymer proposed by Hilt could be programmatically actuated in three steps.[30] This represents an interesting research direction which is worth exploring in the long term.

In this study, we designed and prepared an epoxy-based shape memory (SMEP) multicomposite using four different functional building blocks: a neat SMEP block; SMEP−Fe_3O_4 composite block where the Fe_3O_4 nanoparticles acted as magnetic-responsive phases; SMEP−CNT composite block where the multiwalled carbon nanotubes (MWCNTs) behaved as radiofrequency-responsive phases; and a UV-responsive *p*-aminodiphenylimide-filled SMEP (SMEP-*p*-AP) block, which

Received: September 2, 2017
Accepted: December 4, 2017
Published: December 12, 2017

DOI: 10.1021/acsami.7b13284
ACS Appl. Mater. Interfaces 2017, 9, 44792−44798

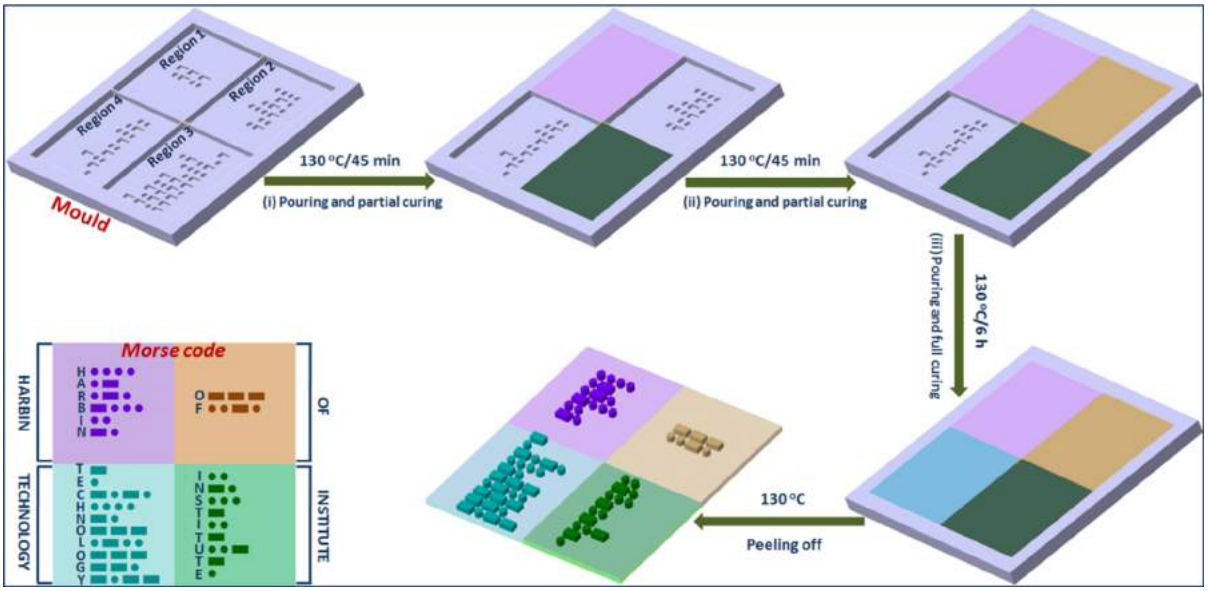

Figure 1. Manufacturing schematic of the surface Morse code patterns on an epoxy-based multicomposite substrate through IL.

allowed us to program regional responses according to a presupposed stimulus procedure. Because of the programmability of temporary shapes, there is a great advantage in introducing Morse code into our fabricated SMEP multicomposite. Here, first, we successfully fabricated four different groups of preprogrammed initial shape memory language code patterns by using step-and-flash imprint lithography at 130 °C. Second, the multicomposite film with permanent code patterns was reprogrammed in a rigid mold cavity which was programmed with a range of round holes using thermal embossing imprint lithography (TE-IL).[31−33] Then, a replica of temporary patterns was obtained after separating from the mold at room temperature. With such a TE-IL reprogramming process, the information passed by language codes can be hidden securely. In addition, the right information passed by code patterns could be obtained by the scheme of the preprogrammed actuation order.

2. EXPERIMENTAL SECTION

2.1. Materials. The SMEP resin in this study was developed by our group.[34] The Fe_3O_4 nanoparticles with a 30 nm average diameter and *p*-aminodiphenylimide (*p*-AP) were commercially available from Aladdin Reagent, China. MWCNTs (length about 30 μm, outer diameter of 20−30 nm) were supplied by Chengdu Institute of Organic Chemistry, China. All chemicals were used as received.

2.2. SMEP Composite Synthesis. First, preweighed fillers (Fe_3O_4, MWCNTs, or *p*-AP) were dispersed in the neat SMEP resin matrix. The filler contents were 5 wt % Fe_3O_4, 0.5 wt % MWCNTs, and 1 wt % *p*-AP. Then, the mixtures were stirred mechanically at room temperature for 0.5 h and ultrasonicated for 15 min. Finally, the mixture was poured into a mold consisting of two glass plates with a 1.5 mm gap. A two-step thermal cure schedule was performed at 100 °C for 3 h and at 130 °C for 6 h. Here, the neat SMEP sample was also prepared for the follow-up characterization and shape memory evaluation.

2.3. Morse Code-Patterned Multicomposite SMEP Synthesis. The Morse code-patterned multicomposite SMEP was synthesized as shown in Figure 1. The four regions were preset with four different Morse codes (region 1: OF; region 2: HARBIN; region 3: TECHNOLOGY; and region 4: INSTITUTE). The four regions were divided by spacing strips to ensure that the corresponding SMEP monomer solution can be reserved in the corresponding region. First, the SMEP-*p*-AP monomer solution and the neat SMEP monomer solution were partially cured for 45 min in regions 1 and 3, respectively. Then, the spacing strips between region 1 and region 2 and between region 2 and region 3 were removed. Afterward, the SMEP−Fe_3O_4 monomer solution was added in region 2 and was also partially cured for 45 min. Second, the spacing strips between region 1 and region 4 and between region 3 and region 4 were removed. After that, the SMEP−CNT monomer solution was added in region 4 and fully cured at 130 °C for 6 h. During the thermal curing process, polymerization of monomer solutions and imprinting of the code patterns were accomplished simultaneously. The multicomposite with language code patterns was obtained after demoulding.

2.4. Characterization. The morphology of SMEP−CNT and SMEP−Fe_3O_4 composites was characterized by a scanning electron microscopy (SEM, Quanta 200, FEI, America) instrument. Differential scanning calorimetry (DSC 1, Mettler-Toledo, Switzerland) was used to test the thermal properties of polymer samples. The specimens were heated from 25 to 200 °C at a rate of 10 °C min^{-1}.

Dynamic mechanical analysis (DMA) was conducted with a DMA Q800 (TA Instruments, USA) instrument. The following conditions were used during the DMA tests: tensile resonant mode, heating rate 5 °C min^{-1}, temperature range 0−200 °C, frequency 1 Hz, and specimen size 29.5 × 2.5 × 1.5 mm (length × width × thickness). Room-temperature static tensile tests were carried out using a universal testing machine (Z010, Zwick/Roell, Germany) at a crosshead speed of 5 mm min^{-1} according to ASTM D638. Three specimens were tested for each material.

2.5. Shape Memory Evaluation. The one-way shape memory cycles were characterized by a DMA Q800 (TA Instruments, USA) instrument with a mode of controlled force. The specimen with a size of 35.5 × 8.5 × 1.5 mm was used. The shape fixity ratio (R_f) was calculated by

$$R_f = \frac{\varepsilon_f}{\varepsilon_{max}} \times 100\% \quad (1)$$

The shape recovery ratio (R_r) was calculated by

$$R_r = \frac{\varepsilon_f - \varepsilon_{ur}}{\varepsilon_f} \times 100\% \quad (2)$$

where ε_{max} is the maximum strain under load, ε_f is the fixed strain after cooling and load release, and ε_{ur} is the unrecovered strain.

2.6. Programmable Morse Code Recovery Demonstration. First, a multicomposite sample with a programmable Morse code pattern-memorizing surface was heated in a 180 °C oven for 10 min.

DOI: 10.1021/acsami.7b13284
ACS Appl. Mater. Interfaces 2017, 9, 44792−44798

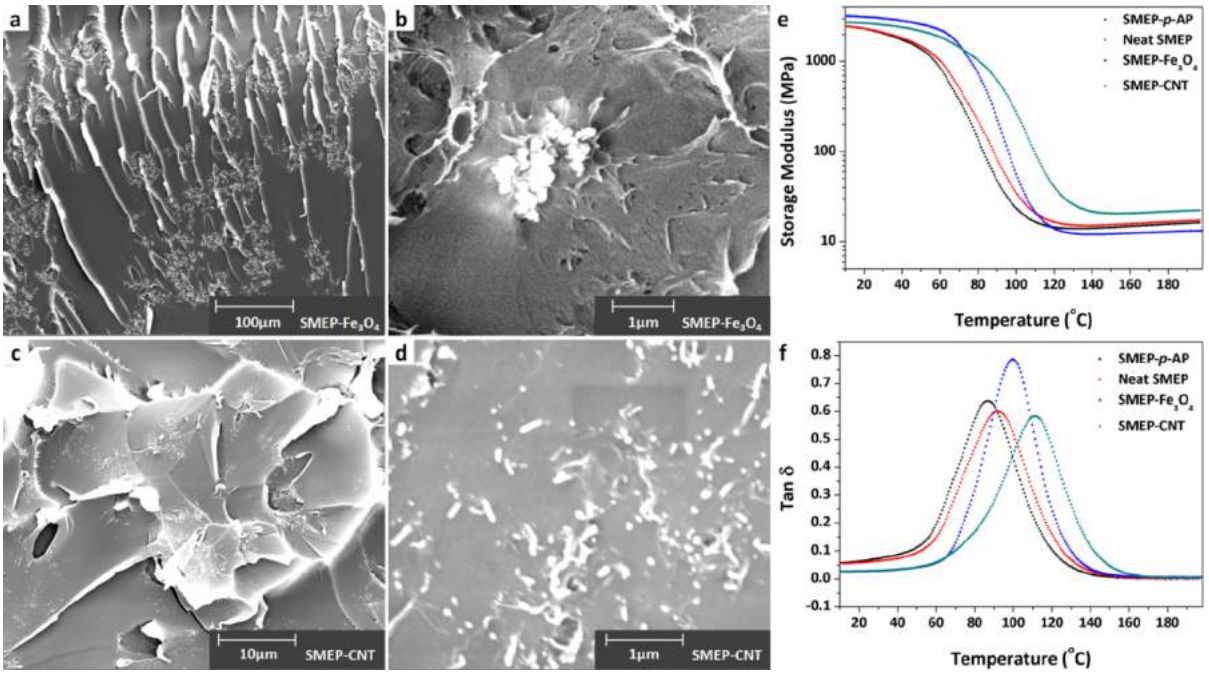

Figure 2. Low-magnification (a) and high-magnification (b) SEM images of the SMEP−Fe_3O_4 composite; low-magnification (c) and high-magnification (d) SEM images of the SMEP−CNT composite; (e) storage modulus E' and (f) loss factor tan δ as a function of the temperature of the SMEP-*p*-AP, neat SMEP, SMEP−Fe_3O_4, and SMEP−CNT specimens tested by DMA.

Then, the four regions with the preprogrammed code patterns on the multicomposite specimen surface were deformed to the temporary patterns with programming mold by TE-IL (8 MPa, 10 min). Second, the multicomposite specimen was cooled to room temperature. After that, it was programmatically exposed to an alternating magnetic field (30 kHz), radiofrequency (rf, 13.56 MHz), UV light (λ = 365 nm), and direct oven heating (130 °C) to display language codes according to the preset command line.

3. RESULTS AND DISCUSSION

3.1. Characterization of Multicomposite SMEP. In this study, the essence of the magnetic response, rf response, and light response of the SMEP composites is thermal actuation. Therefore, the disperse states of Fe_3O_4, MWCNTs, and *p*-AP in the SMEP matrix are important to affect the thermo-mechanical properties and actuation behaviors of the SMEP composites. Because the miscibility of *p*-AP and epoxy is excellent,[35] the cross-section microstructures of the SMEP−Fe_3O_4 and SMEP−CNT composites were first characterized by SEM. From Figure 2a,c, the uniform dispersion was observed for both Fe_3O_4 and MWCNTs at a lower magnification. However, at a higher magnification, the Fe_3O_4 nanoparticles were aggregated into a multiparticle cluster, as shown in Figure 2b, whereas the dispersion of MWCNTs was relatively homogeneous (Figure 2d). The Fe_3O_4 agglomeration was because of its high mass fraction and weak interactions with the SMEP matrix, as similarly reported by Xie and Leng.[30,36]

Figure 2e shows the E' curves versus temperature change of the SMEP composites and neat SMEP analyzed by DMA. With the increase of the temperature, all the specimens showed a degradation of the E' from a high plateau (>2500 MPa) to a low plain of above 13 MPa. The obvious decrease of E' has an enormous contribution to excellent shape memory behaviors.[37] On the other hand, the rubbery modulus (>13 MPa) of the specimens in the elastic state indicated that they could have a high recovery stress in applications.[38] Meanwhile, the tan δ curves (Figure 2f) show that the glass transition temperatures (T_gs) of the neat SMEP, SMEP-*p*-AP, SMEP−Fe_3O_4, and SMEP−CNT composites are 91.8, 86.5, 99.6, and 110.6 °C, respectively. The results of the T_gs increased with the inclusion of Fe_3O_4 and MWCNTs nanoparticles and decreased with the addition of *p*-AP.

The thermal properties of the SMEP composites and neat SMEP were characterized by DSC. From Figure S1 in the Supporting Information, we observed that the T_gs increased with inclusion of Fe_3O_4 and MWCNTs nanoparticles and decreased with the introduction of *p*-AP as compared with the neat SMEP. The T_gs increase may be due to the nanoparticles−SMEP matrix interfacial interactions which can constrain the movements of SMEP chain segments.[39,40] However, The T_g decrease is attributed to the plasticization effect of the *p*-AP molecules.[41,42] Thus, the DSC testing for the four specimens revealed a trend in accordance with the tan δ curves in Figure 2f. However, the DSC results were smaller than the tan δ values; this is due to the fact that the T_g values of polymers depend on the measurement techniques. DSC measures a change in thermodynamic properties (heat capacity) during the glass transition. In comparison, T_g measured from DMA corresponds to the temperature at which the polymer relaxation rate (or segmental relaxation rate) equals the applied frequency. For epoxy-based polymers, the values determined from DSC and DMA can differ by 20 °C.[30,43]

Typical stress−strain curves of the four specimens were tested, and they are shown in Figure S2a in the Supporting Information. As shown in the curves, the maximum tensile strength of neat SMEP was increased by the addition of Fe_3O_4 or MWCNTs and decreased by the introduction of *p*-AP. Meanwhile, Young's modulus (Figure S2b) of the SMEP−Fe_3O_4 and SMEP−CNT composites proved enhancement, and the SMEP-*p*-AP composite proved plasticization. Therefore, the results of Young's modulus also revealed a similar tendency in accordance with the tensile tests shown in Figure S2a.

DOI: 10.1021/acsami.7b13284
ACS Appl. Mater. Interfaces 2017, 9, 44792−44798

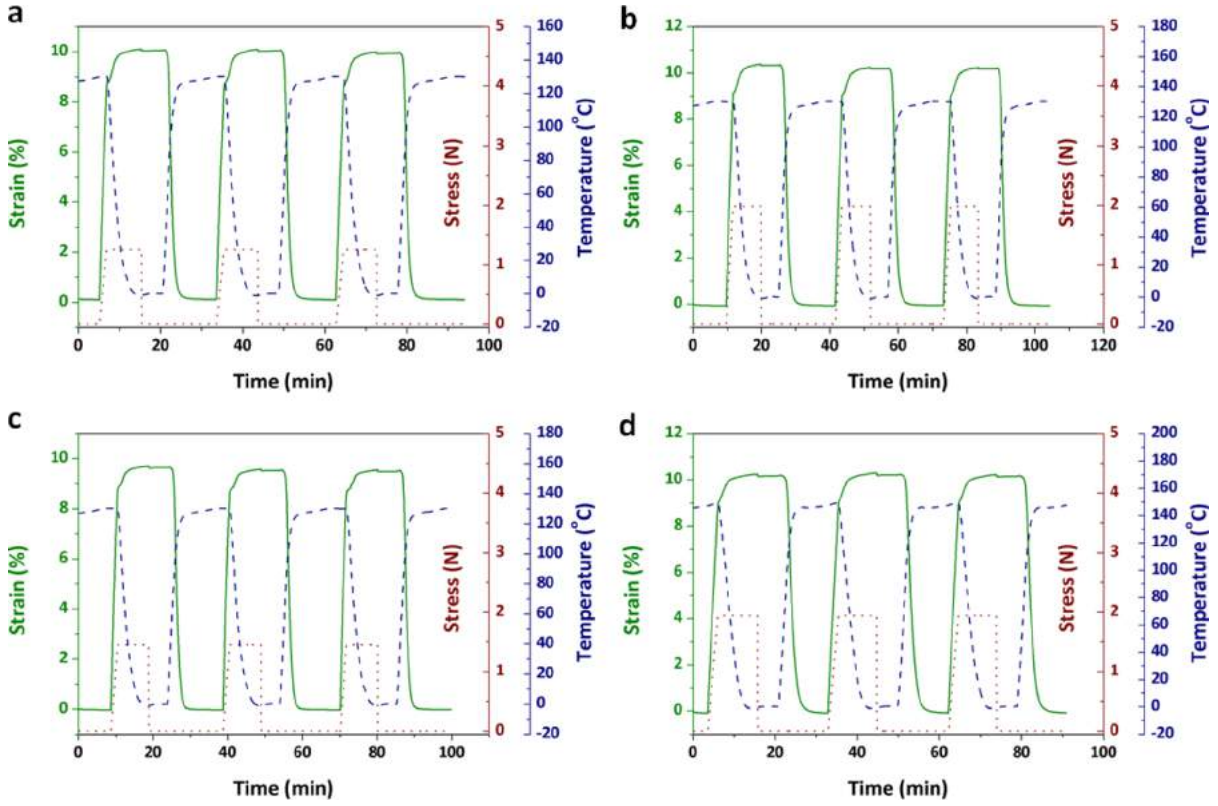

Figure 3. Consecutive one-way shape memory cycles of (a) SMEP-*p*-AP, (b) neat SMEP, (c) SMEP−Fe_3O_4, and (d) SMEP−CNT.

Table S1 shows the detailed mechanical properties of the four specimens. The maximum tensile strengths of SMEP-*p*-AP, neat SMEP, SMEP−Fe_3O_4, and SMEP−CNT are 44.09, 48.29, 59.63, and 66.91 MPa, respectively. In addition, the elongation at break decreases from 46.38 to 11.32%. Herein, we could find that the MWCNTs presented a much better enhancement than the Fe_3O_4 nanoparticles. The reason could be that the tube-shaped MWCNTs with high aspect ratios can reinforce polymers in multidirections, thus offering a better reinforcement than the spherical Fe_3O_4 nanoparticles in the polymer matrix.[44] On the contrary, the introduction of *p*-AP increased the elongation at break of the SMEP polymer matrix. The reason may be that the plasticizing effect of the *p*-AP molecules improved the plastic deformation ability of the SMEP chain segments.[45]

3.2. Investigation of Dual-Shape Memory Properties. The above-mentioned tests (DMA, DSC, and stress−strain) are important to be ready for the evaluation of the shape memory properties of the specimens. Three consecutive shape memory cycles of the four samples (SMEP-*p*-AP, neat SMEP, SMEP−Fe_3O_4, SMEP−CNT) were tested using DMA, and the data are shown in Figure 3a−d. According to the peak values of tan δ curves, we could obtain the T_gs of the specimens. To soften the specimen completely, a higher deformation and recovery temperature (T_g + 40 °C) than T_g was used in the strip-shaped neat SMEP sample according to the previous reports.[46,47] In addition, a higher temperature than T_g was also used for the other three specimens. The values of R_f and R_r for each cycle were calculated from the curves (shown in Figure 3) using eqs 1 and 2. All the specimens displayed high R_f and R_r values above 99%, indicating the excellent ability to maintain the deformed shapes and recover to the original shapes. Taking the neat SMEP (Figure 3b) as an example, the values of R_f for 1st cycle, 2nd cycle, and 3rd cycle are 99.6, 99.6, and 99.5%, respectively. Meanwhile, the values of R_r for 1st cycle, 2nd cycle, and 3rd cycle are 99.6, 99.5, and 99.4%, respectively.

The shape recovery temperatures of the four specimens could be determined by the results of DMA and DSC. The shape recovery processes of SMEP-*p*-AP, neat SMEP, SMEP−Fe_3O_4, and SMEP−CNT specimens with a size of 50 mm × 6 mm × 1.5 mm (length × width × thickness) are exhibited in Figure S3a−d in the Supporting Information. First, the four specimens were heated at 130 °C in the oven for 5 min, fixed to spiral shapes, and then cooled to room temperature under a constraint. After that, the constraint was released, and the temporary shapes were fixed. After keeping the temporary shapes at room temperature for 10 min, the samples were heated to 130 °C again. The spiral specimens of the SMEP-*p*-AP, neat SMEP, SMEP−Fe_3O_4, and SMEP−CNT could recover to their initial shapes in 16, 20, 27, and 35 s, respectively.

3.3. Programmable Recovery of Shape Memory Morse Codes. To realize programmable recovery of the Morse code patterns, the multicomposite specimen which includes an SMEP−Fe_3O_4 region, an SMEP−CNT region, an SMEP-*p*-AP region, and a neat SMEP region was fabricated, and the multistage curing process is shown in detail in the Experimental Section. In the multistage curing processes, the epoxy ensured the strong interfaces among the four regions.[48] We know that the shape memory effect covers many topics, including shape fixity, shape recovery, stress, and strain. Herein, we mainly focused on the programmability of the temporary patterns and the language code recovery process in the shape memory cycle using the preset stimulus command procedure. It can be clearly seen that the recovery route of temporary patterns (reprogramming temporary codes) can be manipu-

DOI: 10.1021/acsami.7b13284
ACS Appl. Mater. Interfaces 2017, 9, 44792−44798

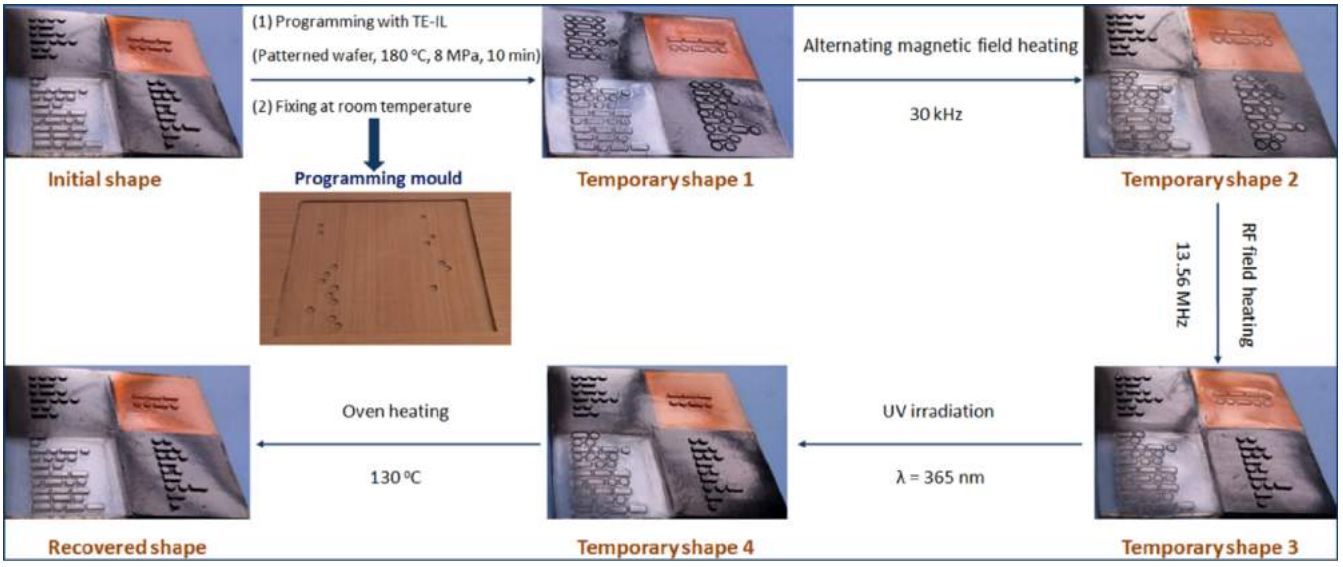

Figure 4. The hiding and programmable recovery of the Morse code patterns. The multicomposite sample was exposed to an alternating magnetic field of 30 kHz, an rf field of 13.56 MHz, a UV irradiation of λ = 365 nm, and a direct oven heating at 130 °C programmatically.

lated by the stimulus order. If the stimulus order is not as our preset command line, then the language code displays information which we do not want to pass.

A multicomposite specimen with raised language code patterns (initial shape) was deformed to the reprogramming temporary patterns (temporary shape 1) in all four regions by TE-IL with a programming mold (consider the illustration in Figure 4), and the code patterns recovery order according to preset command line is experimentally demonstrated in Figure 4. When the multicomposite specimen was exposed to a 30 kHz alternating magnetic field,[36] the SMEP−Fe_3O_4 composite region was heated and the code pattern on this surface was displayed (temporary shape 2), and so we got the first word (HARBIN). When subsequently exposed to a 13.56 MHz rf field,[30,36] the SMEP−CNT composite region was selectively heated and the code pattern on this surface was displayed (temporary shape 3), and hence we got the second word (INSTITUTE). Third, the code pattern on the surface of the SMEP-*p*-AP region recovered after being illuminated by 365 nm UV (temporary shape 4),[35] and then we got the third word (OF). Finally, after being heated in a 130 °C oven, the neat SMEP region was heated and the code pattern of this region appeared (recovered shape). In this case, we got the last word (TECHNOLOGY). Therefore, the information passed by the language codes in the preset stimulus step is "HARBIN INSTITUTE OF TECHNOLOGY". Only in this preset programming stimulus process can we find what information will be passed by language code patterns. If not, you could not get the right information from the irregular code patterns.

4. CONCLUSIONS

In summary, a language code-patterned SMEP multicomposite was prepared through the combination of SMEP−Fe_3O_4, SMEP−CNT, SMEP-*p*-AP, and neat SMEP functional building blocks, and the code patterns were programmed on the four different region surfaces through IL during the thermal curing process. Our method provides excellent compatibility of the four different functional building blocks and results in a multicomposite that has the ability to programmatically actuate code patterns by a preset driver command. Reprogramming pattern transformations in initially raised code patterns was studied in this paper with the purpose of hiding the information passed by the initial language codes. It was observed that the different driver commands could reveal different code information. When the display order was wrong, the information passed by the language codes was also wrong. Hence, our research will contribute to the field of smart information carriers.

■ ASSOCIATED CONTENT

Supporting Information

The Supporting Information is available free of charge on the ACS Publications website at DOI: 10.1021/acsami.7b13284.

DSC thermograms of SMEP-*p*-AP, neat SMEP, SMEP−Fe_3O_4, and SMEP−CNT specimens (Figure S1), tensile results and Young's modulus values of SMEP-*p*-AP, neat SMEP, SMEP−Fe_3O_4, and SMEP−CNT specimens (Figure S2), dual-shape memory recovery processes of SMEP-*p*-AP, neat SMEP, SMEP−Fe_3O_4, and SMEP−CNT specimens (Figure S3), and mechanical properties of SMEP-*p*-AP, neat SMEP, SMEP−Fe_3O_4, and SMEP−CNT specimens (Table S1) (PDF)

■ AUTHOR INFORMATION

Corresponding Author

*E-mail: lengjs@hit.edu.cn.

ORCID

Jinsong Leng: 0000-0001-5098-9871

Notes

The authors declare no competing financial interest.

■ ACKNOWLEDGMENTS

We acknowledge the funding support from National Natural Science Foundation of China (Grant No. 11632005 and 11672086) and Foundation for Innovative Research Groups of the National Natural Science Foundation of China under the grant no. 11421091. The authors also thank Yuanyuan Li and Xin Wang for supporting in the material characterization.

DOI: 10.1021/acsami.7b13284
ACS Appl. Mater. Interfaces 2017, 9, 44792−44798

REFERENCES

(1) Gold, B. Machine Recognition of Hand-Sent Morse Code. *IEEE Trans. Inf. Theory* **1959**, *5*, 17−24.
(2) Schmidt-Wilcke, T.; Rosengarth, K.; Luerding, R.; Bogdahn, U.; Greenlee, M. W. Distinct Patterns of Functional and Structural Neuroplasticity Associated with Learning Morse Code. *NeuroImage* **2010**, *51*, 1234−1241.
(3) Bryan, W. L.; Harter, N. Studies in the Physiology and Psychology of the Telegraphic Language. *Psychol. Rev.* **1897**, *4*, 27−53.
(4) William, L. B.; Harter, N. Studies on the Telegraphic Language: The Acquisition of a Hierarchy of Habits. *Psychol. Rev.* **1899**, *6*, 345−375.
(5) Xu, J.; Song, J. High Performance Shape Memory Polymer Networks Based on Rigid Nanoparticle Cores. *Proc. Natl. Acad. Sci. U.S.A.* **2010**, *107*, 7652−7657.
(6) Behl, M.; Lendlein, A. Shape-Memory Polymers. *Mater. Today* **2007**, *10*, 20−28.
(7) Xie, T. Tunable Polymer Multi-Shape Memory Effect. *Nature* **2010**, *464*, 267−270.
(8) Wei, H.; Zhang, Q.; Yao, Y.; Liu, L.; Liu, Y.; Leng, J. Direct-Write Fabrication of 4D Active Shape-Changing Structures Based on a Shape Memory Polymer and Its Nanocomposite. *ACS Appl. Mater. Interfaces* **2017**, *9*, 876−883.
(9) Zheng, X.; Zhou, S.; Xiao, Y.; Yu, X.; Li, X.; Wu, P. Shape Memory Effect of Poly(D,L-lactide)/Fe_3O_4 Nanocomposites by Inductive Heating of Magnetite Particles. *Colloids Surf., B* **2009**, *71*, 67−72.
(10) Leng, J.; Lan, X.; Liu, Y.; Du, S. Shape-Memory Polymers and Their Composites: Stimulus Methods and Applications. *Prog. Mater. Sci.* **2011**, *56*, 1077−1135.
(11) Pilate, F.; Mincheva, R.; De Winter, J.; Gerbaux, P.; Wu, L.; Todd, R.; Raquez, J.-P.; Dubois, P. Design of Multistimuli-Responsive Shape-Memory Polymer Materials by Reactive Extrusion. *Chem. Mater.* **2014**, *26*, 5860−5867.
(12) Habault, D.; Zhang, H.; Zhao, Y. Light-Triggered Self-Healing and Shape-Memory Polymers. *Chem. Soc. Rev.* **2013**, *42*, 7244−7256.
(13) Li, Z.; Zhang, X.; Wang, S.; Yang, Y.; Qin, B.; Wang, K.; Xie, T.; Wei, Y.; Ji, Y. Polydopamine Coated Shape Memory Polymer: Enabling Light Triggered Shape Recovery, Light Controlled Shape Reprogramming and Surface Functionalization. *Chem. Sci.* **2016**, *7*, 4741−4747.
(14) Li, Y.; Rios, O.; Keum, J. K.; Chen, J.; Kessler, M. R. Photoresponsive Liquid Crystalline Epoxy Networks with Shape Memory Behavior and Dynamic Ester Bonds. *ACS Appl. Mater. Interfaces* **2016**, *8*, 15750−15757.
(15) Chen, Q.; Yu, X.; Pei, Z.; Yang, Y.; Wei, Y.; Ji, Y. Multi-Stimuli Responsive and Multi-Functional Oligoaniline-Modified Vitrimers. *Chem. Sci.* **2017**, *8*, 724−733.
(16) Qi, X.; Yao, X.; Deng, S.; Zhou, T.; Fu, Q. Water-Induced Shape Memory Effect of Graphene Oxide Reinforced Polyvinyl Alcohol Nanocomposites. *J. Mater. Chem. A* **2014**, *2*, 2240−2249.
(17) Liu, C.; Qin, H.; Mather, P. T. Review of Progress in Shape-Memory Polymers. *J. Mater. Chem.* **2007**, *17*, 1543−1558.
(18) Hu, J.; Chen, S. A Review of Actively Moving Polymers in Textile Applications. *J. Mater. Chem.* **2010**, *20*, 3346−3355.
(19) Liu, Y.; Du, H.; Liu, L.; Leng, J. Shape Memory Polymers and Their Composites in Aerospace Applications: A Review. *Smart Mater. Struct.* **2014**, *23*, 023001.
(20) Fritzsche, N.; Pretsch, T. Programming of Temperature-Memory Onsets in a Semicrystalline Polyurethane Elastomer. *Macromolecules* **2014**, *47*, 5952−5959.
(21) Pretsch, T.; Ecker, M.; Schildhauer, M.; Maskos, M. Switchable Information Carriers Based on Shape Memory Polymer. *J. Mater. Chem.* **2012**, *22*, 7757−7766.
(22) Ecker, M.; Pretsch, T. Durability of Switchable QR Code Carriers Under Hydrolytic and Photolytic Conditions. *Smart Mater. Struct.* **2013**, *22*, 094005.
(23) Ecker, M.; Pretsch, T. Multifunctional Poly(ester urethane) Laminates with Encoded Information. *RSC Adv.* **2014**, *4*, 286−292.
(24) Zarek, M.; Layani, M.; Cooperstein, I.; Sachyani, E.; Cohn, D.; Magdassi, S. 3D Printing of Shape Memory Polymers for Flexible Electronic Devices. *Adv. Mater.* **2016**, *28*, 4449−4454.
(25) Zhao, Q.; Qi, H. J.; Xie, T. Recent Progress in Shape Memory Polymer: New Behavior, Enabling Materials, and Mechanistic Understanding. *Prog. Polym. Sci.* **2015**, *49*, 79−120.
(26) Yakacki, C. M.; Shandas, R.; Safranski, D.; Ortega, A. M.; Sassaman, K.; Gall, K. Strong, Tailored, Biocompatible Shape-Memory Polymer Networks. *Adv. Funct. Mater.* **2008**, *18*, 2428−2435.
(27) Koerner, H.; Price, G.; Pearce, N. A.; Alexander, M.; Vaia, R. A. Remotely Actuated Polymer Nanocomposites-Stress-Recovery of Carbon-Nanotube-Filled Thermoplastic Elastomers. *Nat. Mater.* **2004**, *3*, 115−120.
(28) Meng, H.; Li, G. A Review of Stimuli-Responsive Shape Memory Polymer Composites. *Polymer* **2013**, *54*, 2199−2221.
(29) Wu, Y.; Hu, J.; Zhang, C.; Han, J.; Wang, Y.; Kumar, B. A Facile Approach to Fabricate a UV/Heat Dual-Responsive Triple Shape Memory Polymer. *J. Mater. Chem. A* **2015**, *3*, 97−100.
(30) He, Z.; Satarkar, N.; Xie, T.; Cheng, Y.-T.; Hilt, J. Z. Remote Controlled Multishape Polymer Nanocomposites with Selective Radiofrequency Actuations. *Adv. Mater.* **2011**, *23*, 3192−3196.
(31) Wang, Z.; Hansen, C.; Ge, Q.; Maruf, S. H.; Ahn, D. U.; Qi, H. J.; Ding, Y. Programmable, Pattern-Memorizing Polymer Surface. *Adv. Mater.* **2011**, *23*, 3669−3673.
(32) Cox, L. M.; Killgore, J. P.; Li, Z.; Zhang, Z.; Hurley, D. C.; Xiao, J.; Ding, Y. Morphing Metal-Polymer Janus Particles. *Adv. Mater.* **2014**, *26*, 899−904.
(33) Cox, L. M.; Sun, X.; Wang, C.; Sowan, N.; Killgore, J. P.; Long, R.; Wu, H.-A.; Bowman, C. N.; Ding, Y. Light-Stimulated Permanent Shape Reconfiguration in Cross-Linked Polymer Microparticles. *ACS Appl. Mater. Interfaces* **2017**, *9*, 14422−14428.
(34) Leng, J.; Wu, X.; Liu, Y. Effect of a Linear Monomer on the Thermomechanical Properties of Epoxy Shape-Memory Polymer. *Smart Mater. Struct.* **2009**, *18*, 095031.
(35) Yu, L.; Wang, Q.; Sun, J.; Li, C.; Zou, C.; He, Z.; Wang, Z.; Zhou, L.; Zhang, L.; Yang, H. Multi-Shape-Memory Effects in a Wavelength-Selective Multicomposite. *J. Mater. Chem. A* **2015**, *3*, 13953−13961.
(36) Li, W.; Liu, Y.; Leng, J. Selectively Actuated Multi-Shape Memory Effect of a Polymer Multicomposite. *J. Mater. Chem. A* **2015**, *3*, 24532−24539.
(37) Yu, X.; Zhou, S.; Zheng, X.; Guo, T.; Xiao, Y.; Song, B. A Biodegradable Shape-Memory Nanocomposite with Excellent Magnetism Sensitivity. *Nanotechnology* **2009**, *20*, 235702.
(38) Xie, T.; Xiao, X. Self-Peeling Reversible Dry Adhesive System. *Chem. Mater.* **2008**, *20*, 2866−2868.
(39) Abdalla, M.; Dean, D.; Adibempe, D.; Nyairo, E.; Robinson, P.; Thompson, G. The Effect of Interfacial Chemistry on Molecular Mobility and Morphology of Multiwalled Carbon Nanotubes Epoxy Nanocomposite. *Polymer* **2007**, *48*, 5662−5670.
(40) Gu, H.; Tadakamalla, S.; Huang, Y.; Colorado, H. A.; Luo, Z.; Haldolaarachchige, N.; Young, D. P.; Wei, S.; Guo, Z. Polyaniline Stabilized Magnetite Nanoparticle Reinforced Epoxy Nanocomposites. *ACS Appl. Mater. Interfaces* **2012**, *4*, 5613−5624.
(41) Li, W.; Liu, Y.; Leng, J. Shape Memory Polymer Nanocomposite with Multi-Stimuli Response and Two-Way Reversible Shape Memory Behavior. *RSC Adv.* **2014**, *4*, 61847−61854.
(42) Li, W.; Gong, T.; Chen, H.; Wang, L.; Li, J.; Zhou, S. Tuning Surface Micropattern Features Using a Shape Memory Functional Polymer. *RSC Adv.* **2013**, *3*, 9865−9874.
(43) Castro, F.; Westbrook, K. K.; Hermiller, J.; Ahn, D. U.; Ding, Y.; Qi, H. J. Time and Temperature Dependent Recovery of Epoxy-Based Shape Memory Polymers. *J. Eng. Mater. Technol.* **2011**, *133*, 021025.
(44) Xu, B.; Fu, Y. Q.; Ahmad, M.; Luo, J. K.; Huang, W. M.; Kraft, A.; Reuben, R.; Pei, Y. T.; Chen, Z. G.; De Hosson, J. T. M. Thermo-Mechanical Properties of Polystyrene-Based Shape Memory Nanocomposites. *J. Mater. Chem.* **2010**, *20*, 3442−3448.

DOI: 10.1021/acsami.7b13284
ACS Appl. Mater. Interfaces 2017, 9, 44792−44798

(45) Kulinski, Z.; Piorkowska, E. Crystallization, Structure and Properties of Plasticized Poly(L-lactide). *Polymer* **2005**, *46*, 10290−10300.
(46) Pandini, S.; Baldi, F.; Paderni, K.; Messori, M.; Toselli, M.; Pilati, F.; Gianoncelli, A.; Brisotto, M.; Bontempi, E.; Riccò, T. One-Way and Two-Way Shape Memory Behaviour of Semi-Crystalline Networks Based on Sol-Gel Cross-Linked Poly(ε-caprolactone). *Polymer* **2013**, *54*, 4253−4265.
(47) Yang, X.; Wang, L.; Wang, W.; Chen, H.; Yang, G.; Zhou, S. Triple Shape Memory Effect of Star-Shaped Polyurethane. *ACS Appl. Mater. Interfaces* **2014**, *6*, 6545−6554.
(48) Xie, T.; Xiao, X.; Cheng, Y.-T. Revealing Triple-Shape Memory Effect by Polymer Bilayers. *Macromol. Rapid Commun.* **2009**, *30*, 1823−1827.

NOTE ADDED AFTER ASAP PUBLICATION

This paper published ASAP on 12/12/2017. The Supporting Information was corrected and the revised version was reposted on 12/13/2017.

DOI: 10.1021/acsami.7b13284
ACS Appl. Mater. Interfaces 2017, 9, 44792−44798